Spectroelectrochemistry of Silver Deposition on Single Gold Nanocrystals

ARTICLE *in* JOURNAL OF PHYSICAL CHEMISTRY LETTERS · NOVEMBER 2014

Impact Factor: 7.46 · DOI: 10.1021/jz502349x

4 AUTHORS, INCLUDING:

Mariana Chirea
Koc University
21 PUBLICATIONS **312** CITATIONS
SEE PROFILE

Sean S. E. Collins
University of Melbourne
7 PUBLICATIONS **30** CITATIONS
SEE PROFILE

Paul Mulvaney
University of Melbourne
311 PUBLICATIONS **24,741** CITATIONS
SEE PROFILE

THE JOURNAL OF PHYSICAL CHEMISTRY Letters

Letter

pubs.acs.org/JPCL

Spectroelectrochemistry of Silver Deposition on Single Gold Nanocrystals

Mariana Chirea,*[,†,¶] Sean S. E. Collins,[‡] Xingzhan Wei,[‡] and Paul Mulvaney*[,‡]

[†]CIQ-L4, Faculdade de Ciências, Universidade do Porto, Rua do Campo Alegre, 687, 4169-007 Porto, Portugal

[‡]School of Chemistry and Bio21 Institute, University of Melbourne, Parkville, Victoria 3010, Australia

Supporting Information

ABSTRACT: We report the electrodeposition of metallic silver onto gold nanostars adsorbed to ITO electrodes. The electrochemical process was studied at the single particle level by correlated in situ dark field spectroscopy and scanning electron microscopy (SEM). Underpotential deposition avoids bulk silver formation on the ITO substrates. SEM proves that deposition occurs on all surfaces of the gold nanostars when polyvinylpyrrolidone (PVP) is stabilizing the nanostars or preferentially at the nanostar tips when the ligand is removed. The surface plasmon resonance blue-shifts by more than 100 nm following the formation of a 5 nm Ag film on PVP stabilized gold nanostars, moving the scattered color from the near-infrared to red or orange. The spectral shifts can be accurately modeled using finite element simulations. These results demonstrate that the morphology and composition of individual bimetallic nanocrystals can be engineered electrochemically.

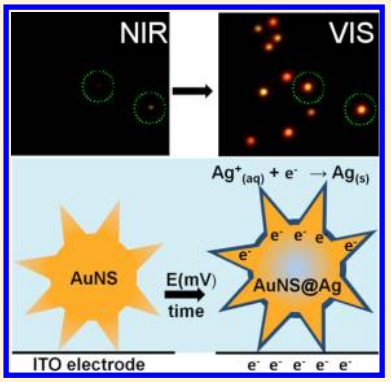

SECTION: Plasmonics, Optical Materials, and Hard Matter

The study of catalytic processes and redox reactions on metal nanocrystal surfaces is extremely challenging. Rates of reaction are highly sensitive to a variety of parameters including the particle size and shape, the degree of crystal faceting, the occurrence of underpotential deposition and the role of substrate interactions.[1] These factors are all convoluted in ensemble electrochemical measurements,[2−7] and consequently, one approach for obviating these problems is to study redox processes on single metal nanoparticles.[8−11]

Underpotential deposition (UPD) refers to formation of metal adatoms and adlayers at potentials more positive than the equilibrium redox potential.[12−16] It is an important phenomenon in electrochemistry and has been exploited for decades to grow monolayer metal films.[12−16] It has also been used in the past as a means to grow core−shell metal nanocrystals[17] and is implicated in the formation mechanism of anisotropic gold particles from gold seeds.[18] Here, we use real-time spectroelectrochemistry to study the underpotential deposition of silver onto single gold nanocrystals for the first time. The gold particles are adsorbed to a conducting indium tin oxide (ITO) substrate. Normally, the adsorbed gold particles and ITO substrate are at a common electrochemical potential and metal deposition should occur homogeneously over the entire surface. Electrochemical nucleation and deposition generally on a variety of metal electrodes has been shown to lead to polydisperse, dendritic particle formation.[19,20] Indeed, previous groups have shown that the application of large cathodic potentials to ITO electrodes immersed in $AgNO_3$ solution leads to indiscriminate nucleation and uncontrolled, though spectacular, growth of silver particles on ITO substrates.[19] Conversely, our goal here is to show that highly selective deposition of silver atoms onto gold nanocrystals is possible without concomitant bulk nucleation and growth on the ITO substrate. This enables the electrochemistry of single metal particles to be studied. We have selected gold nanostars (AuNSs) for the deposition process because they are multifaceted—the sharp needle-like structures are likely to promote metal deposition—but also because they exhibit sharp, intense surface plasmon resonances in the visible part of the spectrum or NIR region. Furthermore, the polyvinylpyrrolidone layer that colloidally stabilizes the AuNSs forms complexes with Ag^{+} ions in solution, which may also facilitate the deposition of Ag adatoms and adlayers.[21] Gold nanostars and other nanoparticle morphologies have previously been employed as plasmon binding sensors in a dark field microscope (DFM),[22−25] but there are no reports on nanostar electrochemical properties at the single particle level.

We carried out chronoamperometry at very low silver ion concentrations (<1 μM) in 0.1 M $NaNO_3$ as supporting electrolyte. Deposition of silver was accompanied by strong blue shifts of the localized surface plasmon resonance (LSPR) of the gold nanostars, which was used to monitor the electrochemical process. Electron microscopy was used to prove that deposition occurred onto the nanostars and to determine the surface coverage of silver. The gold nanostars were synthesized via seed mediated growth in *N*,*N*-

Received: November 5, 2014
Accepted: November 29, 2014
Published: November 29, 2014

dimethylformamide (DMF) using poly(*N*-vinylpyrrolidone) (PVP) as a colloidal stabilizer.[25] Full experimental details, including nanocrystal synthesis, electrode preparation and single particle spectroelectrochemical setup are provided in the Supporting Information file.

In Figure 1a, the localized surface plasmon resonance (LSPR) peak position (red markers) is plotted as a function of time during an applied cathodic potential sequence ranging between 0 mV and −100 mV (blue trace).

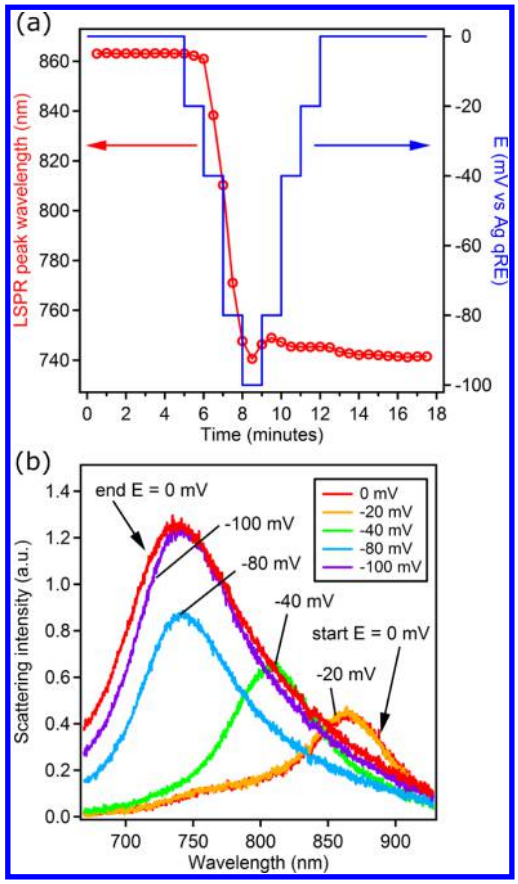

Figure 1. (a) Position of the surface plasmon band peak of a single gold nanostar as a function of both time (red circles) and the applied potential (blue line), measured during electrodeposition of metallic silver from 6.7×10^{-7} M $AgNO_3$ and 0.1 M $NaNO_3$ aqueous solution. (b) Selected Rayleigh scattering spectra of the same gold nanostar collected at various applied potentials during the deposition process. The nanostar was coated with PVP.

The potential was initially held constant at 0 mV relative to the quasi-Ag reference electrode for 5 min prior to the application of the potential step sequence. During this time, the LSPR peak position was stable (±1 nm) and this indicates that there was no silver ion reduction at this potential. After the initial preconditioning of the system at 0 mV, a series of increasingly cathodic potential steps was applied. Scattering spectra were collected at each potential. Note that each spectrum required a 30 s acquisition time and the potential was held constant at each value for at least 60 s to enable two spectra to be acquired. It is evident that at 0 mV and −20 mV, the LSPR peak position and scattering intensities remained unchanged (red and orange spectra, start potential in Figure 1b). Then at −40 mV, silver deposition started to occur and the LSPR blue-shifted 51 nm in 60 s and there was a concomitant 45% increase in the scattering intensity (green spectrum in Figure 1b). At $E = -100$ mV, there was a 122 nm blue shift of the LSPR and the scattering intensity had increased to 2.6 times the original value (purple spectrum in Figure 1b). The silver was not readily reoxidized, as shown by the stable position of the LSPR peak when the potential was returned back to 0 V (Figure 1a).

Real-time video DFM footage of the nanostar growth process is provided in the Supporting Information file. Two very different types of electrochemical behavior were observed both by video and spectroscopically. Gold nanostars that had been imaged in the SEM prior to voltammetry measurements did not undergo silver deposition (they are noted in the video by "area with marked nanostars", see also Supporting Information Figure S2), whereas gold nanostars unexposed to the electron beam prior to reaction did undergo Ag deposition (in the video, Ag deposition on unexposed AuNSs is demonstrated by color and intensity changes that begin at −40 mV, which is confirmed by DFM spectra presented in Figure 1b and Supporting Information Figure S4). In the case of preimaged AuNSs, we believe the electron beam carbonizes the PVP coating, resulting in a carbon shell that passivates the Au surface and prevents silver deposition from occurring (Supporting Information Figure S2). Contrarily, on unexposed gold nanostars, there is a change in shape from star to a more flower-like structure with thicker cores and tips (Supporting Information Figure S3). This effect of the SEM rendered the collection of images of the same individual nanostars before and after electrochemical coating impossible.

To circumvent this issue, a protocol for removal of the PVP coating was developed. The AuNSs were spin coated onto ITO working electrodes (second setup described in the Supporting Information file) and pretreated with a 0.04 M sodium borohydride ($NaBH_4$) solution for 15 min in order to remove the PVP.[26] Silver electrodeposition on these "bare" AuNSs was performed by using 5×10^{-7} M $AgNO_3$ and 0.1 M $NaNO_3$ aqueous solution (Figure 2, Supporting Information Figures S5−S8). The deposition process was slower under these conditions (Supporting Information Figure S5). As before, there were no evident changes in spectra at the open circuit potential or at 0 mV applied potential. Small −20 mV cathodic steps were then applied to the ITO for 60 s. From Supporting Information Figure S5, it can be seen that the gold nanostar underwent a very slight blue shift of 2 nm at −20 mV, demonstrating that silver was already being deposited at this potential. A slight increase in deposition rate occurred when the potential was changed to −160 mV and the LSPR peak blue-shifted 5 nm. After the potential was held at −160 mV for 8 min, the applied potential was further reduced to −180 mV (8 min), −200 mV (8 min), and −220 mV (1 min). At each new potential, the rate of blue shift initially increased again, then slowed but never stopped. This indicates that at each of these potentials there was a steady-state flux of silver to the nanostar, and electrochemical equilibrium was never achieved. In Figure 2a, the final scattering spectrum of the Ag covered Au nanostar after the total 40 min sequence is shown (blue line) as well as the initial spectrum (red line). The total blue shift in the scattering spectrum of this single nanostar over the 40 min sequence was 31 nm, and there was a 30% increase in the scattering intensity. A control experiment was carried out under the same experimental conditions without any added $AgNO_3$ to confirm that the LSPR shift was caused by the silver ions (green plot, Supporting Information Figure S5).

dx.doi.org/10.1021/jz502349x | *J. Phys. Chem. Lett.* 2014, 5, 4331−4335

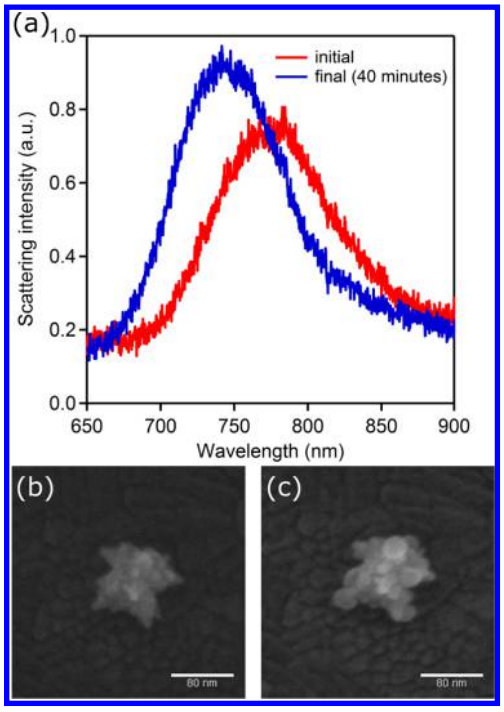

Figure 2. (a) Full scattering spectra of a single, $NaBH_4$-treated nanostar at the open circuit potential before (red) and after (blue) electrodeposition of metallic silver from 5×10^{-7} M $AgNO_3$ and 0.1 M $NaNO_3$ aqueous solution at potentials varying from 0 mV to −220 mV. (b, c) SEM image of the same nanostar as in panel a before (b) and after (c) Ag deposition.

The blue shifts in the scattering spectra occur at very small cathodic biases. However, such blue shifts may also be due to double-layer charging or potential induced shape changes to the particles. To resolve these contributions, again we carried out SEM imaging on the nanostars before and after chronoamperometry to determine whether they retain their star-like morphology.

In Figure 2b and c, we present two images of the same gold nanostar before and after the electrodeposition process. The nanostar had been treated with $NaBH_4$ and the postdeposition image clearly exhibits a change in morphology due to the deposited silver. This is the same particle for which the optical data shown in Figure 2a were obtained. In this case, the silver appears to be deposited predominantly on the tips as spheres or agglomerates,[27,28] with little change to the overall size of the particle. Furthermore, no indiscriminate nucleation of Ag on the adjacent ITO surface was visible. This absence of "free" silver nucleation was observed for all samples (see, e.g., Supporting Information Figures S6−S8). This result differs significantly from literature reports. Ag shelling on Au nanostars[29] and nanorods[30] stabilized in solution occurs via epitaxial growth on low energy crystal facets due to the presence of surfactants and halide ions.[31] Conversely here, the dominant factor controlling the spatial distribution of the deposited silver is the local electrical double layer at "bare" metal nanostars, because the electric field is highest near the tips, enhancing migration of silver ions. Our work demonstrates that electrochemical deposition of Ag is dependent only on applied potential, time of reaction, and presence or absence of the stabilizing ligand at the nanocrystal surface. Our procedure is simpler compared with the chemical deposition of silver on gold crystals which is highly dependent on temperature, pH of solution, reducing agent, stabilizing ligand, and interference of competing products such as AgCl or AgBr.[29−32]

In Figure 3a, we present calculations of the predicted spectral shifts of the nanostar LSPR during silver deposition. We simulated the nanostars as spheres with eight projecting conical protuberances, to match the SEM images. COMSOL software was used to calculate the scattering cross section of the particles for even coatings of silver on the surface. A homogeneous dielectric constant of $\varepsilon_m = 1.78$ for the environment was assumed. The COMSOL simulations predict a blue shift of 120 nm similar to the experimentally observed shifts of 122 nm for PVP stabilized nanostars that had not been exposed to the electron beam. Figure 3b illustrates the charge distribution on a silver coated gold nanostar during illumination at 729 nm, corresponding to the major scattering peak. These charge distributions reveal that the major LSP resonance is a dipolar resonance. Figure 3c demonstrates how well the relationship between the increase in relative scattering intensity and blue shift matches for the theoretical and experimental data. This close match allows us to predict the thickness of the silver shell throughout the deposition process. The thicknesses are calculated to range from as little as a monolayer of approximately 0.2 nm up to 5 nm thick coatings under the conditions employed in these experiments. From the volume change in the particles determined by SEM, we estimate that there is deposition of 1.8×10^6 silver atoms in 150 s. Assuming that the flux is controlled by the interfacial transfer rate, we may

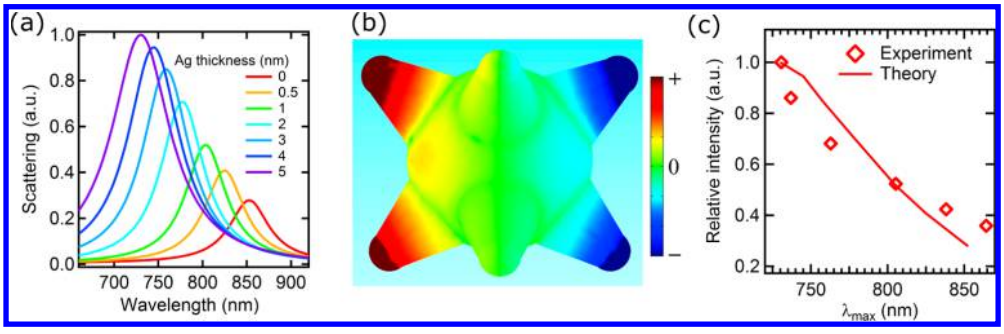

Figure 3. (a) Calculated scattering spectra using COMSOL of a gold nanostar with different homogeneous Ag shell thicknesses, assuming $\varepsilon_m = 1.78$. Dielectric data for gold is from ref 33. (b) Calculated surface charge distribution at the major, dipolar scattering peak $\lambda = 729$ nm. Diameter of the gold sphere core, 57 nm; tip length, 27 nm; length of tip base, 23 nm; radius of tip apex, 2.5 nm; refractive index of the surrounding medium, 1.33. (c) Plot of the relative intensity of the LSPR peak as a function of the peak wavelength of the LSPR band during silver deposition. Diamonds are experimental data and continuous line is the fit from COMSOL simulations.

dx.doi.org/10.1021/jz502349x | J. Phys. Chem. Lett. 2014, 5, 4331−4335

write J (mol/s) = $4\pi R^2 k_{et}$[Ag]. Inserting R = 28.5 nm and [Ag] = 6.7 μM yields $k_{et} \sim 0.3$ cm/s, which corresponds to a moderate heterogeneous rate constant, but this indicates that deposition of silver is occurring well below the diffusion limit. Under these conditions, the spatial distribution of silver will be controlled by the double layer structure as assumed above.

In summary, we have shown that with fine control of the applied potential close to the reversible potential of Ag^+/Ag, controlled deposition of silver onto individual gold nanostars can be achieved. The resulting scattering spectrum of the gold−silver core−shell particle can be tuned over 100 nm by deposition of just 1−5 nm of silver. Additionally, we found that electron beam imaging has a drastic effect on the surface chemistry of the nanostars by carbonizing the PVP ligand. Chemical pretreatment with sodium borohydride removes the PVP but changes the kinetics of Ag electrodeposition. The absence of PVP also promotes Ag deposition primarily on the tips of the Au nanostars generating bimetallic nanostructures.

■ ASSOCIATED CONTENT

Ⓢ Supporting Information

Materials and methods, chemical synthesis of gold nanostars, additional results containing SEM images of AuNS@Ag nanostructures, additional spectroelectrochemical measurements, and a movie of the electrochemical reaction of homogeneous shelling conditions. This material is available free of charge via the Internet at http://pubs.acs.org.

■ AUTHOR INFORMATION

Corresponding Authors

*E-mail: mariana.chirea@uvigo.es.

*E-mail: mulvaney@unimelb.edu.au.

Present Address

¶Departamento de Química Física, Universidade de Vigo, 36310 Vigo, Spain.

Notes

The authors declare no competing financial interest.

■ ACKNOWLEDGMENTS

M.C. gratefully acknowledges financial support for the travel to Australia from Fardin Derogarian and Iwona Biernacka. P.M. thanks the ARC for support under Grant LF 100100117 and the Melbourne Centre for Nanofabrication for access under the Technology Fellowship program. Support through U.S. AOARD Grant 134016 is also appreciated.

■ REFERENCES

(1) Daniel, M. C.; Astruc, D. Gold Nanoparticles: Assembly, Supramolecular Chemistry, Quantum-Size-Related Properties, and Applications toward Biology, Catalysis, and Nanotechnology. *Chem. Rev.* **2004**, *104*, 293−346.

(2) Talapin, D. V.; Lee, J. S.; Kovalenko, M. K.; Shevchenko, E. V. Prospects of Colloidal Nanocrystals for Electronic and Optoelectronic Applications. *Chem. Rev.* **2010**, *110*, 389−458.

(3) Chirea, M. Electron Transfer at Gold Nanostar Assemblies: A Study of Shape Stability and Surface Density Influence. *Catalysts* **2013**, *3*, 288−309.

(4) Chirea, M.; Garcia-Morales, V.; Manzanares, J. A.; Pereira, C. M.; Gulaboski, R.; Silva, F. Electrochemical Characterization of Polyelectrolyte/Gold Nanoparticle Multilayers Self-Assembled on Gold Electrodes. *J. Phys. Chem. B* **2005**, *109*, 21808−21817.

(5) Chirea, M.; Pereira, C. M.; Silva, F. Catalytic Effect of Gold Nanoparticles Self-Assembled in Multilayered Polyelectrolyte Films. *J. Phys. Chem. C* **2007**, *111*, 9255−9266.

(6) Chirea, M.; Cruz, A.; Pereira, C. M.; Silva, F. Size-Dependent Electrochemical Properties of Gold Nanorods. *J. Phys. Chem. C* **2009**, *113*, 13077−13087.

(7) Chirea, M.; Borges, J.; Pereira, C. M.; Silva, F. Density-Dependent Electrochemical Properties of Vertically Aligned Gold Nanorods. *J. Phys.Chem. C* **2010**, *114*, 9478−9488.

(8) Novo, C.; Funston, A. M.; Gooding, A. K.; Mulvaney, P. Electrochemical Charging of Single Gold Nanorods. *J. Am. Chem. Soc.* **2009**, *131*, 14664−4666.

(9) Li, Y.; Cox, J. T.; Zhang, B. Electrochemical Responses and Electrocatalysis at Single Au Nanoparticles. *J. Am. Chem. Soc.* **2010**, *132*, 3047−3054.

(10) Olson, J.; Dominguez-Medina, S.; Hoggard, A.; Wang, L. Y.; Chang, W. S.; Link, S. Optical Characterization of Single Plasmonic Nanoparticles. *Chem. Soc. Rev.* **2014**, DOI: 10.1039/c4cs00131a.

(11) Byers, C. P.; Hoener, B. S.; Chang, W.-S.; Yorulmaz, M.; Link, S.; Landes, C. F. Single-Particle Spectroscopy Reveals Heterogeneity in Electrochemical Tuning of the Localized Surface Plasmon. *J. Phys. Chem. B* **2014**, DOI: 10.1021/jp504454y.

(12) Herrero, E.; Buller, L. J.; Abruna, H. D. Underpotential Deposition at Single Crystal Surfaces of Au, Pt, Ag and Other Materials. *Chem. Rev.* **2001**, *101*, 1897−1930.

(13) Jennings, G.; Laibinis, P. E. Self-Assembled *n*-Alkanethiolate Monolayers on Underpotentially Deposited Adlayers of Silver and Copper on Gold. *J. Am. Chem. Soc.* **1997**, *119*, 5208−5214.

(14) Shimazu, K.; Kawaguchi, T.; Isomura, T. Construction of Mixed Mercaptopropionic Acid/Alkanethiol Monolayers of Controlled Composition by Structural Control of a Gold Substrate with Underpotentially Deposited Lead Atoms. *J. Am. Chem. Soc.* **2002**, *124*, 652−661.

(15) Takami, S.; Jennings, G. K.; Laibinis, P. E. Composite Monolayer of Ag and Cu on Au(111) by Sequential Underpotential Deposition. *Langmuir* **2001**, *17*, 441−448.

(16) Nishizawa, M.; Sunagawa, T.; Yoneyama, H. Underpotential Deposition of Copper on Gold Electrodes through Self-Assembled Monolayers of Propanethiol. *Langmuir* **1997**, *13*, 5215−5217.

(17) Price, S. W. T.; Speed, J. D.; Kannan, P.; Russell, E. A. Exploring the First Steps in Core−Shell Electrocatalyst Preparation: In Situ Characterization of the Underpotential Deposition of Cu on Supported Au Nanoparticles. *J. Am. Chem. Soc.* **2011**, *133*, 19448−19458.

(18) Personick, M. L.; Langille, M. R.; Zhang, J.; Mirkin, C. A. Shape Control of Gold Nanoparticles by Silver Underpotential Deposition. *Nano Lett.* **2011**, *11*, 3394−3398.

(19) Ueda, M.; Dietz, H.; Anders, A.; Kneppe, H.; Meixner, A.; Plieth, W. Double-Pulse Technique as an Electrochemical Tool for Controlling the Preparation of Metallic Nanoparticles. *Electrochim. Acta* **2002**, *48*, 377−386.

(20) Tian, N.; Zhou, Z. Y.; Sun, S. G.; Cui, L.; Ren, B.; Tian, Z. Q. Electrochemical Preparation of Platinum Nanothorn Assemblies with High Surface Enhanced Raman Scattering Activity. *Chem. Commun.* **2006**, 4090−4092.

(21) Yin, B.; Ma, H.; Wang, S.; Chen, S. Electrochemical Synthesis of Silver Nanoparticles under Protection of Poly(*N*-vinylpyrrolidone). *J. Phys. Chem. B* **2003**, *107*, 8898−8904.

(22) Dondapati, S. K.; Sau, T. K.; Hrelescu, C.; Klar, T. A.; Stefani, F. D.; Feldmann, J. Label-free Biosensing Based on Single Gold Nanostars as Plasmonic Transducers. *ACS Nano* **2010**, *4*, 6318−6322.

(23) Baciu, C. L.; Becker, J.; Janshoff, A.; Sonnichsen, C. Protein−Membrane Interaction Probed by Single Plasmonic Nanoparticles. *Nano Lett.* **2008**, *8*, 1724−1728.

(24) Khalavka, Y.; Becker, J.; Sonnichsen, C. Synthesis of Rod-Shaped Gold Nanorattles with Improved Plasmon Sensitivity and Catalytic Activity. *J. Am. Chem. Soc.* **2009**, *131*, 1871−1875.

(25) Barbosa, S.; Agrawal, A.; Rodriguez-Lorenzo, L.; Pastoriza-Santos, I.; Alvarez-Puebla, R. A.; Kornowski, A.; Weller, H.; Liz-Marzan, L. M. Tuning Size and Sensing Properties in Colloidal Gold Nanostars. *Langmuir* **2010**, *26*, 14943−14950.

(26) Ansar, S. M.; Ameer, F. S.; Hu, W.; Zou, S.; Pittman, C. U.; Zhang, D. Removal of Molecular Adsorbates on Gold Nanoparticles Using Sodium Borohydride in Water. *Nano Lett.* **2013**, *13*, 1226−1229.
(27) Hill, C. M.; Pan, S. A Dark-Field Scattering Spectroelectrochemical Technique for Tracking the Electrodeposition of Single Silver Nanoparticles. *J. Am. Chem. Soc.* **2013**, *135*, 17250−17253.
(28) Hill, C. M.; Clayton, D. A.; Pan, S. Combined Optical and Electrochemical Methods for Studying Electrochemistry at the Single Molecule and Single Particle Level: Recent Progress and Perspectives. *Phys. Chem. Chem. Phys.* **2013**, *15*, 20797−20807.
(29) Samal, A. K.; Polavarapu, L.; Sergio Rodal-Cedeira, S.; Liz-Marzan, L. M.; Perez-Juste, J.; Pastoriza-Santos, I. Size Tunable Au@Ag Core−Shell Nanoparticles: Synthesis and Surface-Enhanced Raman Scattering Properties. *Langmuir* **2013**, *29*, 15076−15028.
(30) Xiang, Y.; Wu, X.; Liu, D.; Li, Z.; Chu, W.; Feng, L.; Zhang, K.; Zhou, W.; Xie, S. Gold Nanorod-Seeded Growth of Silver Nanostructures: From Homogeneous Coating to Anisotropic Coating. *Langmuir* **2008**, *24*, 3465−3470.
(31) Gomez-Grana, S.; Goris, B.; Altantzis, T.; Fernandez-Lopez, C.; Carbo-Argibay, E.; Guerrero-Martinez, A.; Almora-Barrios, N.; Lopez, N.; Pastoriza-Santos, I.; Perez-Juste, J. Au@Ag Nanoparticles: Halides Stabilize {100} Facets. *J. Phys. Chem. Lett.* **2013**, *4*, 2209−2216.
(32) Rodriguez-Gonzalez, B.; Burrows, A.; Watanabe, M.; Kiely, C. J.; Liz-Marzan, L. M. Multishell Bimetallic AuAg Nanoparticles: Synthesis, Structure and Optical Properties. *J.Mater. Chem.* **2005**, *15*, 1755−1759.
(33) Johnson, P. B.; Christy, R. W. Optical Constants of the Noble Metals. *Phys. Rev. B* **1972**, *6*, 4370−4379.